APL Materials

RESEARCH ARTICLE | MAY 10 2023

Complex magnetic ordering behavior in the frustrated perovskite Ba_2MnMoO_6

Special Collection: Challenges and Perspectives in Materials Chemistry—A Celebration of Prof. Sir Anthony K. Cheetham's 75th Birthday

Fiona C. Coomer; Heather M. Mutch; Otto Mustonen; ... et. al

APL Mater 11, 051111 (2023)
https://doi.org/10.1063/5.0144719

Complex magnetic ordering behavior in the frustrated perovskite Ba_2MnMoO_6

Cite as: APL Mater. 11, 051111 (2023); doi: 10.1063/5.0144719
Submitted: 31 January 2023 • Accepted: 24 March 2023 •
Published Online: 10 May 2023

Fiona C. Coomer,[1] Heather M. Mutch,[2] Otto Mustonen,[3] Charlotte Pughe,[2] Serena A. Cussen[2] Silvia Ramos,[4] Adrian D. Hillier,[5] and Edmund J. Cussen[2,a)]

AFFILIATIONS

[1] Echion Technologies, Sawston, Cambridge DB22 3FQ, United Kingdom
[2] Department of Materials Science and Engineering, University of Sheffield, Sheffield S1 3JD, United Kingdom
[3] School of Chemistry, University of Birmingham, Edgbaston, Birmingham B15 2TT, United Kingdom
[4] School of Physics and Astronomy, University of Kent, Canterbury CT2 7NH, United Kingdom
[5] ISIS Pulsed Neutron and Muon Source, STFC Rutherford Appleton Laboratory, Didcot OX11 0QX, United Kingdom

Note: This paper is part of the Special Topic on Challenges and Perspectives in Materials Chemistry—A Celebration of Prof. Sir Anthony K. Cheetham's 75th Birthday.

[a)] **Author to whom correspondence should be addressed:** e.j.cussen@sheffield.ac.uk

ABSTRACT

New and exotic ground states of magnetic materials are highly sought after and are extensively studied for the insights they provide into the thermodynamics of disorder and fundamental magnetic interactions. By controlling the crystal structure of an appropriate magnetic lattice, it is possible to cause the strong magnetic exchange interactions to sum to zero and so be frustrated. Due to the presence of this frustration, the lowest energy configuration that results may be crucially dependent on the tiniest of energy differences between a multitude of states that have (almost) the same energy. The keen interest in these materials arises from the fact that these finely balanced systems offer a way of probing classical or quantum mechanical interactions that are of fundamental importance but are too weak to be observed in non-frustrated systems. Here, we combine local and crystallographic probes of the cation-ordered double perovskite Ba_2MnMoO_6 that contains a face-centered cubic lattice of S = 5/2 Mn^{2+} cations. Neutron diffraction measurements below 9.27(7) K indicate that a fourfold degenerate non-collinear antiferromagnetic state exists with almost complete ordering of the Mn^{2+} spins. Muon spin relaxation measurements provide a local probe of the magnetic fields inside this material over the $t_{1/2}$ = 2.2 μs lifetime of a muon, indicating a slightly lower Néel transition temperature of 7.9(1) K. The *dc* susceptibility data do not show the loss of magnetization that should accompany the onset of the antiferromagnetic order; they indicate that a strongly antiferromagnetically coupled paramagnetic state [θ = −73(3) K] persists down to 4 K, at which temperature a weak transition occurs. The behavior of this material differs considerably from the closely related compositions Ba_2MnMO_6 (M = W, Te), which show collinear ordering arrangements and well defined antiferromagnetic transitions in the bulk susceptibility. This suggests that the Mo^{6+} cation leads to a fine balance between the nearest and next-nearest neighbor superexchange in these frustrated double perovskite structures.

INTRODUCTION

Geometric magnetic frustration arises when there are magnetic interactions that cannot all be simultaneously satisfied in a system, and it is most commonly found in lattice systems containing antiferromagnetic interactions that form triangular motifs.[1] In order to relieve this frustration, the magnetic moments often order in a non-collinear arrangement such that there is no net moment around a particular plaquette or they undergo a structural distortion as[2] in MnO to favor conventional ordering. There has been a significant amount of recent research interest in finding insulating magnetic materials containing geometrically frustrated antiferromagnetic interactions.[3–8] The presence of competing interactions in such materials can lead to the suppression of the long-range

order and so allow the emergence of exotic ground states. These include the spin liquid ground state proposed by Anderson,[9–11] spin glass,[12–14] spin ice,[15,16] and valence bond glass ground states,[4,17,18] based on triangular, kagome, pyrochlore, and face-centered cubic (*fcc*) lattices. Of these, the *fcc* lattice, consisting of edge sharing tetrahedra, has historically attracted less attention, although it has enjoyed a recent resurgence in interest[19] due to the discovery of a valence bond glass state in Ba_2YMoO_6 and Ba_2LuMoO_6.[4,17,18,20] The *B*-site cation-ordered double perovskite structure with the general formula $A_2BB'O_6$, where both the *B* and *B*′ sites form interpenetrating *fcc* lattices, affords a physical realization of this frustrated lattice, as shown in Fig. 1. Unfortunately, physical examples of undistorted *fcc* lattices in double perovskites are rare due to the great degree of structural diversity arising from distortions and tilting of the octahedra, relieving the frustration by lifting the degeneracy of the interactions.[21]

The current interest in S = 1/2 magnetic systems on the *fcc* lattice[19,22–24] has been driven by the combination of low spin values and frustration leading to unusual quantum magnetic states such as the valence bond glass in $BaYMoO_6$ and $BaLuMoO_6$.[4,17,18,20] As part of a program to investigate the Jahn–Teller activity of Mo^{5+} in Ba_2NdMoO_6[25] by doping with Mn,[26] we have reinvestigated the behavior of Mn^{2+} cations forming an undistorted *fcc* lattice.[27,28]

High spin Mn^{2+} has long been considered as a model ion for the study of the magnetic behavior,[29,30] most clearly illustrated in the rock salt structured *fcc* lattice of MnO that provided the first demonstration[31] of long-range antiferromagnetic type ordering of spins as predicted by Néel.[32,33] The behavior of Mn^{2+} on *fcc* lattices has continued to provide new insights into the complex interplay of structure and spin ordering to illuminate our understanding of the magnetic behavior.[2] Here, we report our study of the same spherical high spin d^5, Mn^{2+}, wherein we adjust the magnetic interactions by arranging it within a cation ordered perovskite. Although a chemically different structure, this provides exactly the same *fcc* topology as the archetypal MnO system; in terms of lattice geometry, frustration, and magnetic moment anisotropy, it is a direct analog of this prototypical material.

Although Ba_2MnMoO_6 is a well-known material,[34–36] the magnetic properties are more complex than has hitherto been appreciated. The related compounds Ba_2MnTeO_6[27] and Ba_2MnWO_6[28] show well-defined transitions in magnetic susceptibility that is coincidental with the appearance of magnetic Bragg peaks in the neutron diffraction profile indicative of long-range antiferromagnetism of type I and type II orderings, respectively. Here, we show that in the apparently similar compound Ba_2MnMoO_6, the transition temperature shows a more complex behavior that shows a distinct technique dependence. Ba_2MnMoO_6 shows well defined magnetic Bragg peaks in the diffracted thermal neutron wave, but the magnetic susceptibility does not show the well-defined maxima observed in Ba_2MnWO_6 and Ba_2MnTeO_6. Muon spin relaxation measurements in Ba_2MnMoO_6 characterize a sharp magnetic transition that drastically differs from Ba_2MnWO_6 and Ba_2MnTeO_6 systems, where correlations persist up to temperatures five times greater than T_N. These results show that unusual magnetic properties can still be discovered in classical magnetic systems and that these double perovskites merit further re-investigation.

METHODS

Sample preparation

Polycrystalline Ba_2MnMoO_6 was prepared by the solid state reaction of stoichiometric quantities of $BaCO_3$ (99.997%), MnO_2 (99.999%), and MoO_3 (99.998%). These were intimately ground together and pressed into pellets. The pellets were heated in air from 500 to 800 °C at 1 °C min^{-1} and held at 800 °C for 8 h to prevent the volatilization of Mo. After grinding and re-pelleting, the pellets were heated at 1250 °C in flowing 5% H_2/N_2. Further regrinding and reheating were performed until phase purity was confirmed by

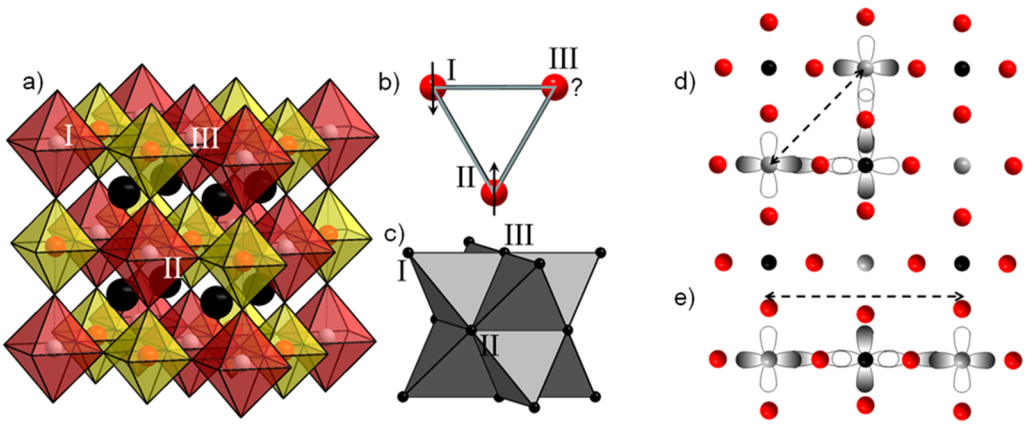

FIG. 1. (a) Face-centered cubic perovskite lattice is formed by cation ordering between Mn^{2+} and Mo^{6+} onto the larger and smaller MO_6 octahedral sites indicated by red and yellow octahedra, respectively. An equilateral triangle is formed by the nearest neighboring Mn^{2+} cations, and panel (b) illustrates the geometric frustration of antiferromagnetic coupling between them. Panel (c) shows the lattice points on the *fcc* lattice of Mn spins on positions labeled as I, II, and III in each diagram. The nearest neighbor interaction between Mn^{2+} cations, illustrated as gray spheres in (d), has the shortest through-space interaction. However, the superexchange pathway is mediated by the orbital overlap and the distance between next-nearest spins shown in (e) has the same through-bond distance as the nearest neighbor interaction in (d).

laboratory powder x-ray diffraction. The same sample was used for all property measurements reported here. Repeats of x-ray diffraction and SQUID magnetometry measurements on samples from repeat syntheses showed no significant variation.

Magnetometry measurements

d.c. susceptibility measurements were performed using Quantum Design MPMS SQUID magnetometers. A polycrystalline sample (50 mg) was mounted in a gelatin capsule and measured in an applied field of 1000 G after cooling in both zero applied field (ZFC) and an applied field of 1000 G (FC). Calculations of the diamagnetic correction showed that this had a negligible contribution to the susceptibility, and so this correction was not applied. These measurements were repeated using three different magnetometers and three different samples. No significant variation was observed for any of these data.

a.c. susceptibility measurements were performed at frequencies of 2, 10, and 20 Hz in a RMS field of 1 G in the temperature range $2 \leq T/K \leq 45$.

Neutron powder diffraction

Low temperature neutron powder diffraction measurements were performed at the Institut Laue-Langevin (ILL) in Grenoble using the high-resolution diffractometer D2B using an incident neutron wavelength of 1.5935 Å, and variable temperature measurements were performed using the high flux diffractometer D1B (incident wavelength 2.5214 Å). The samples were contained in cylindrical vanadium cans, and the temperature was controlled using an orange cryostat. Rietveld refinements against the data were performed using the GSAS suite of programs,[37,38] using a pseudo-Voigt peak shape and a shifted Chebyshev background function.

X-ray absorption

Temperature dependent extended x-ray absorption fine structure (EXAFS) measurements were performed on Ba_2MnMoO_6 at the Mo K-edge, using the B18 beamline at the Diamond Light Source and processed and analyzed using the Athena and Artemis packages.[39,40]

Muon spin relaxation

μSR measurements were performed using the MuSR instrument at the ISIS Pulsed Neutron and Muon Source, at Rutherford Appleton Laboratories in the UK. The powdered sample was mounted on a 99.995+% pure silver plate, covered with a kapton foil and contained in a standard ^{4}He cryostat. The calibration constant for these measurements was determined by the application of a 20 G transverse magnetic field to determine the relaxation function. Data were collected in longitudinal configuration and analyzed using the Mantid software package.[41]

RESULTS

Susceptibility measurements

Bulk d.c. magnetization measurements (Fig. 2) on Ba_2MnMoO_6 are in agreement with previous reports[35] and show Curie–Weiss paramagnetism at high temperatures ($T \geq 150$ K). Fits to the data yield a Curie constant, $C = 5.21(5)$ emu mol^{-1} K^{-1}, and a Weiss temperature, $\theta = -73(3)$ K, indicating strong antiferromagnetic coupling between high spin $S = 5/2$, Mn^{2+} cations. Despite the strong antiferromagnetic interactions, only a small cusp in the susceptibility is observed at 4 K, and there is minimal divergence of FC and ZFC susceptibility. This slight downturn in susceptibility would correspond to a frustration factor $f = \frac{|\theta|}{T_N} = 18$[1] but is not indicative of a bulk cancellation of spins as is seen in conventional antiferromagnetic double perovskites.[25] Repeat measurements using freshly prepared Ba_2MnMoO_6 indicated no variation in the magnetization behavior. a.c. susceptibility data showed no frequency dependence and showed a similar maximum at 4 K as shown in Fig. 2.

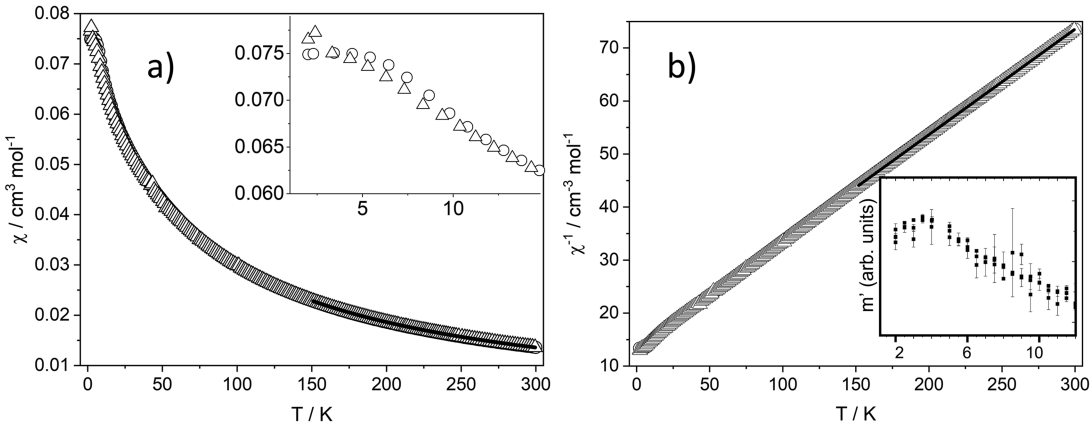

FIG. 2. (a) *d.c.* susceptibility of Ba_2MnMoO_6 measured in an applied field of 1000 G after cooling in zero field (Δ) and in 1000 G (○). The solid line shows a fit to the Curie–Weiss law for $T \geq 150$ K with the parameter $C = 5.21(5)$ emu mol^{-1} K^{-1} and a Weiss temperature, $\theta = -73(3)$ K. The inset shows the low temperature data. (b) The inverse susceptibility shows the agreement between the Curie–Weiss law and the data. The inset shows that the in-phase component (m') of the *a.c.* magnetization with data collected at 2, 10, and 20 Hz is invariant with frequency and typically are within 1 standard deviation as indicated by the error bars.

High resolution neutron powder diffraction

The formation of a single phase cation-ordered perovskite was followed using laboratory x-ray diffraction. This provides a good estimate of cation ordering due to the large scattering contrast between Mn (Z = 25) and Mo (Z = 42), and the final crystallographic analysis used data from the high resolution diffractometer D2B. This use of neutrons allows reliable assessment of the oxide ion parameters that are less well determined by x rays in the presence of dominant x-ray scatterers, such as Ba and Mo. Moreover, it gives excellent contrast between the scattering lengths of Mn^{2+} (−0.373 fm) and Mo^{6+} (6.715 fm). Rietveld refinement against the high resolution neutron diffraction data showed complete cation ordering over the two octahedral sites in the structure. This is in keeping with previous studies of this composition and is unsurprising, given the difference in cation charge, cation radius ($r_{Mn}{}^{2+}$ = 0.83 Å and $r_{Mo}{}^{6+}$ = 0.59 Å),[42] and the resultant large difference in the size of the two octahedral sites indicated by the large difference in bond lengths of 2.157 Å and 1.925 Å.

High resolution neutron diffraction datasets were collected at temperatures of 25 and 1.5 K. The 25 K data could be refined in the cubic space group $Fm\bar{3}m$ [a = 8:16 470(5) Å] with Mn and Mo fully ordered on the B sites. Multiple test refinements showed full occupancy of all crystallographic sites; i.e., there is no oxygen deficiency. On cooling to 1.5 K, there was no evidence of a structural phase transition and the nuclear Bragg reflections are indexed in the same cubic space group [a = 8:16 305(5) Å]. Despite this, a number of additional peaks were observed, which could be indexed using a cubic magnetic cell with $a_{mag} = 2a_{nuc}$, indicative of the long-range antiferromagnetic order with a propagation vector of $\mathbf{k} = \left(\frac{1}{2}, \frac{1}{2}, \frac{1}{2}\right)$. Initially, these magnetic peaks were fitted using a collinear model[43] (Fig. 3), which gave a reasonable agreement [X^2 = 4.44, R_{wp} = 7.64, Mn moment = 4.16(10) μ_B]. This type II magnetic structure is similar to that observed in monoclinically distorted MnO[2] and the cubic double perovskite Ba_2MnWO_6.[28] The absence of a maximum in the susceptibility of Ba_2MnMoO_6 provides a sharp contrast to the obvious signature of conventional antiferromagnetic ordering observed in Ba_2MnWO_6. This led us to consider alternative origins for the magnetic Bragg scattering, and so a number of other models were tested.

To develop a model, we considered the coupling between the next nearest neighbor Mn^{2+} spins, as although the through-space distance of the interactions is longer than that for the nearest neighbor interaction, the through-bond (Mn–O–Mo–O–Mn) distance is identical, as shown in Fig. 1. These interactions are often dominant in double perovskites where both B-site cations are transition metals, for example, La_2CoRuO_6 and Sr_2CoOsO_6.[24,44,45] The through-bond interaction is dominant in Sr_2CoOsO_6, which contains two interpenetrating *fcc* lattices of paramagnetic cations Co, $3d^7$, and Os, $5d^2$.

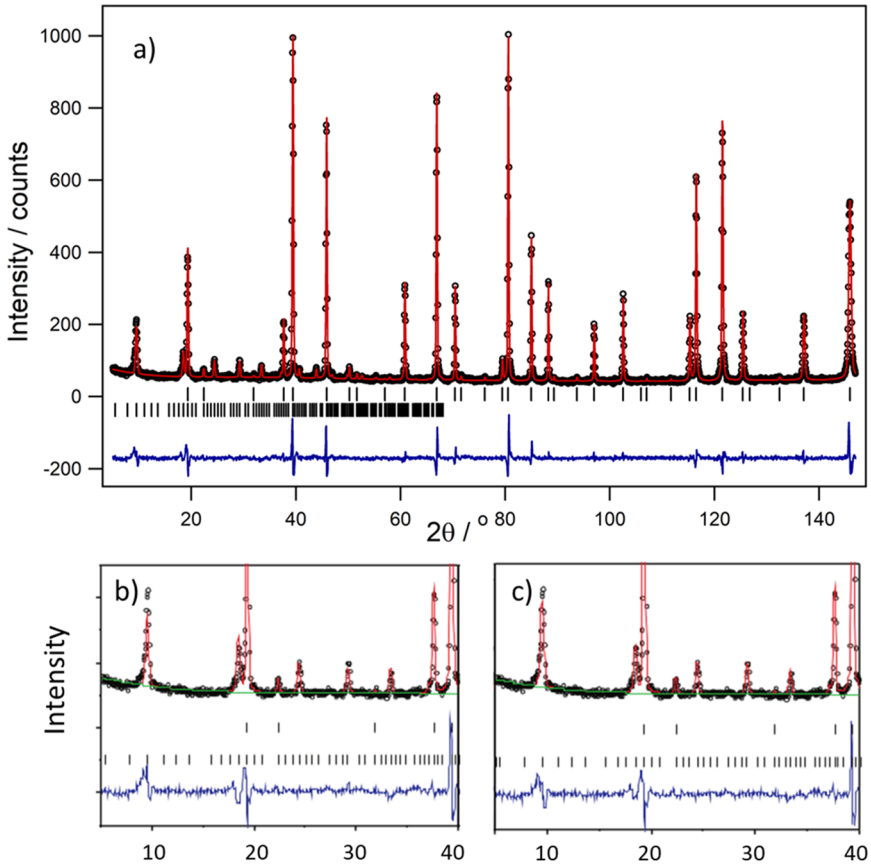

FIG. 3. Rietveld refinement of the nuclear (upper tick marks) and magnetic (lower tick marks) structure of Ba_2MnMoO_6 against neutron powder diffraction data collected at 1.5 K on the D2B diffractometer. Crystal data: $Fm\bar{3}m$, a = 8.16305(5) Å, Ba(8c), U_{iso} = −0.0005(8), Mn (4a) U_{iso} = −0.0004(5), Mo (4b) U_{iso} = −0.0004(5), O(24e) x = 0.2642(3), U_{11} = 0.0028(9), and $U_{22,33}$ = 0.0037(6). The upper plot (a) shows the entire data range, and the bottom plots show the low angle data refined against (b) the type II magnetic structure and (c) the non-collinear arrangement of spins.

Due to the difference in energy between these 3d and 5d orbitals, there is only very weak coupling via the nearest Co–O–Os interaction and two separate interpenetrating magnetic structures result, where the strongest coupling occurs via the exchange between cobalt atoms.[24,45] Considering these next nearest neighbor interactions allows the magnetic lattice to be viewed as four interpenetrating sublattices, as highlighted by Anderson.[46] The spins within each of these sublattices can be coupled forming a G-type antiferromagnetic structure. If each of these sublattices has spins orientated along a different one of the four ⟨111⟩ directions, a structure containing spin-compensated tetrahedra is created, as shown in Fig. 4. The dominance of the intra-sublattice coupling over the inter-sublattice coupling leads to a ground state exhibiting macroscopic degeneracy. This structure is consistent with the undistorted cubic-structure, and refinement of this structure against the low temperature neutron powder diffraction data results in a slight improvement in the quality of fit [X^2 = 4.19, R_{wp} = 7.42, Mn moment = 3.87(8) μ_B].

Temperature dependent magnetic Bragg scattering

To study the evolution of the magnetic structure, the temperature dependence of these magnetic peaks was investigated using the D1B diffractometer, at temperatures spanning both paramagnetic and antiferromagnetic regimes. The data were fitted using refinement of both the nuclear and magnetic structures. The variation in the unit cell parameter of the nuclear cell as a function of temperature is plotted in Fig. 5. As expected, the unit cell contracts on cooling to T ≈ 20 K, but negative thermal expansion is observed on cooling below this temperature. At 1.5 K, the refined manganese magnetic moment is in agreement with that expected for a fully antiferromagnetically ordered Mn^{2+} moment. On heating toward T_N, the refined moment decreases, and in the region of T_N (Fig. 5), this could be fitted using a standard function[47] for the critical exponent, β, of the sublattice magnetization: $\mu_{Mn} = A\left(\frac{T_N - T}{T_N}\right)^{\beta}$. Fits over the temperature range close to T_N (4.75 ≤ T ≤ 9.2 K) yielded the parameters T_N = 9.37(7) K and β = 0.38(2). This value of β is consistent

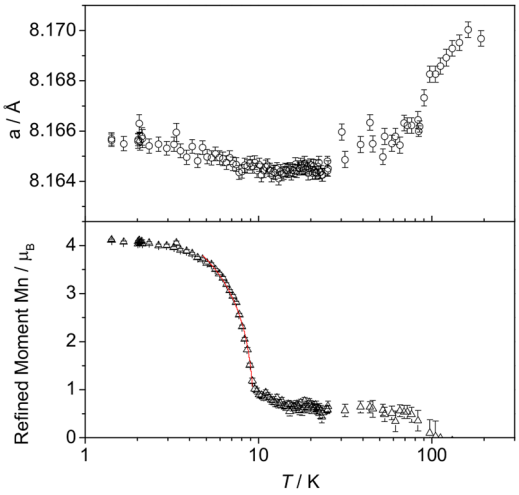

FIG. 5. Temperature dependence of (a) the nuclear cubic unit cell parameter and (b) the refined manganese magnetic moment of Ba_2MnMoO_6 measured on the high flux diffractometer D1B. The red line in the bottom panel shows a fit of the critical exponent, T_N = 9.37(7) K and β = 0.38(2). The error bars indicate the estimated standard deviation derived from Rietveld refinements. The inset shows the temperature dependence of the magnetic Bragg peaks in the neutron diffraction data collected using the D1B diffractometer.

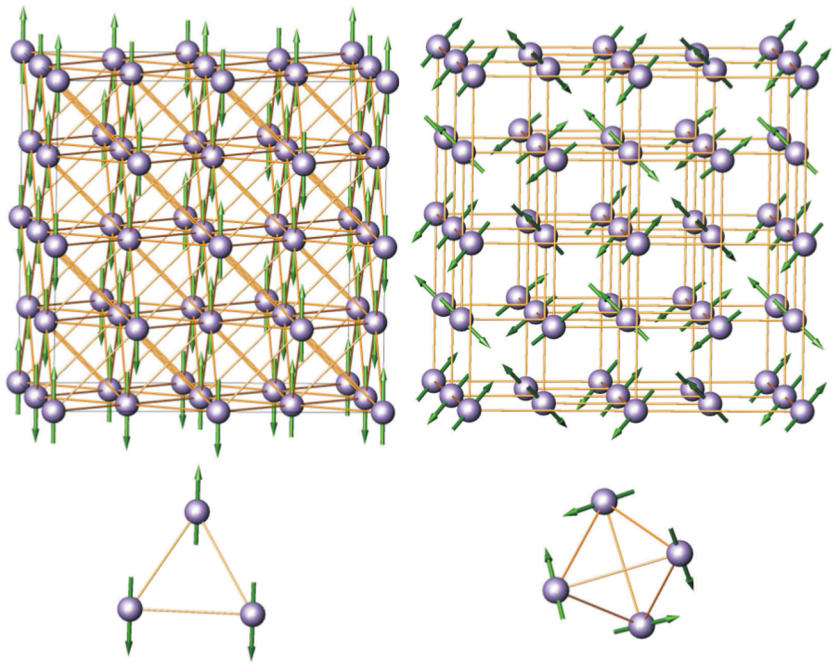

FIG. 4. Proposed magnetic structures of Ba_2MnMoO_6 using the type II structure (left) and spin compensated tetrahedra (right). The lines indicate the magnetic exchange pathways between the moments on the Mn^{2+} cations.

TABLE I. Parameters obtained from refinements against EXAFS data for Ba_2MnMoO_6. All data were fitted simultaneously using a common, temperature independent value for E_0.

Parameters	1.5 K	60 K	160 K	300 K
S_0^2Mo	0.85(4)	0.85(4)	0.85(4)	0.85(4)
E_0	−4.7(8)	−4.7(8)	−4.7(8)	−4.7(8)
R Mo–O (N = 6)	1.921(9)[a]	1.919(6)	1.921(6)	1.923(8)
σ^2 Mo–O (N = 6)	0.003(1)	0.0024(6)	0.0024(7)	0.003(1)
R Mo–Ba (N = 8)	3.544(5)[a]	3.547(3)	3.549(5)	3.55(1)
σ^2 Mo–Ba (N = 8)	0.0016(4)	0.0018(3)	0.0030(4)	0.0051(9)
R Mo–O–Mn (N = 12)	4.09(1)[a]	4.099(7)	4.11(1)	3.99(3)
σ^2 Mo–O–Mn (N = 12)	0.003(9)	0.0030(6)	0.0039(9)	0.012(7)

[a]These interatomic distances can be compared with the values derived from Rietveld refinements against neutron diffraction data collected at 1.5 K: Mo···O 1.925 Å, Mo···Ba 3.535 Å, and Mo···Mn 4.082 Å.

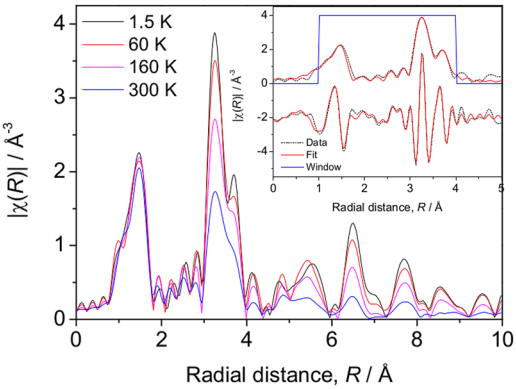

FIG. 6. Temperature dependence of the magnitude of the Fourier transform of the EXAFS data measured at four characteristic temperatures: 1.5, 60, 160, and 300 K. Inset: fits against the magnitude (upper) and real component (lower) of the Fourier transform in real space (R) of the EXAFS spectrum measured at 1.5 K. The data are shown by the broken lines, and the fits are shown by the solid red lines. The blue line represents the fitting range of 1–4 Å.

with that expected for 3D ordering of an Heisenberg antiferromagnet,[47] supporting the assignment that the magnetic ordering is, indeed, 3D in nature, rather than the 2D exponent expected for ordering in sheets. These neutron diffraction data unambiguously demonstrate that almost all the Mn^{2+} moments are incorporated into the macroscopically degenerate long-range ordered antiferromagnetic structure with a T_N significantly higher than that observed by *d.c.* susceptibility. Using the ordering temperature determined from neutron diffraction gives a frustration factor f of ~8 that is significantly lower than the value of 18 inferred from bulk susceptibility measurements.

Local probe of the structure

Temperature dependent EXAFS measurements were performed at the Mo K-edge in order to investigate the local coordination environment and oxidation state of the molybdenum ion. The position of the K-edge in these measurements confirms that molybdenum is present in the diamagnetic Mo(VI) oxidation state, thus confirming that the only magnetic species is S = 5/2, Mn^{2+}. These findings are in agreement with the result of calculations[34] that indicate Ba_2MnMoO_6 is an insulator containing Mo^{6+} and Mn^{2+}. The EXAFS data measured at 1.5, 60, 160, and 300 K were simultaneously fitted constraining common values, to calculate the local environment about the Mo^{6+} cation. An R range of 1–4 Å and a k range of 2.727–15.608 $Å^{-1}$ were used. A good fit to all the data could be obtained using the cubic structure from the low temperature neutron diffraction data as a starting model. The details of the fit are shown in Table I. The fit to the data measured at 1.5 K is shown in the inset of Fig. 6. There is no evidence of distortion of the frustrated

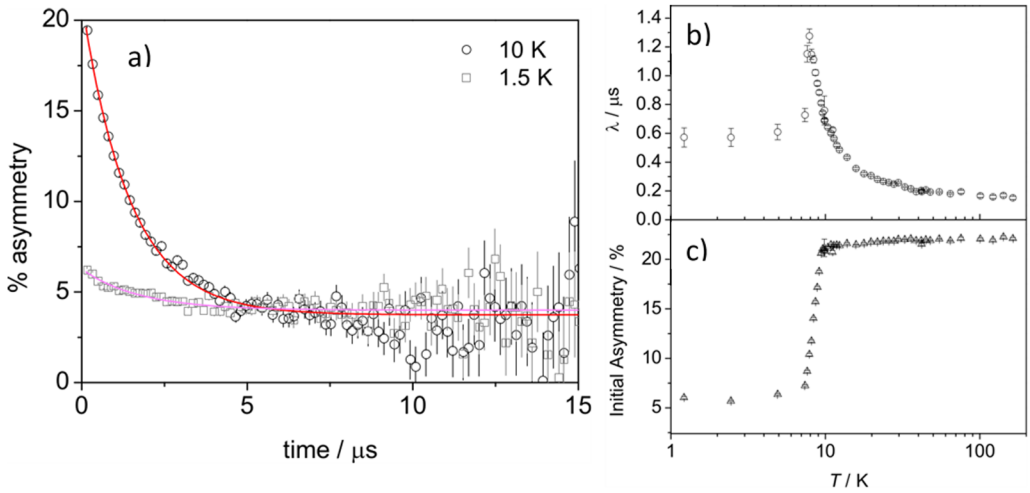

FIG. 7. (a) Zero field μSR data measured above (black circles) and below (gray squares) T_N with the lines showing their associated fits to an exponential relaxation. The temperature dependence of (b) the relaxation rate, λ, and (c) the initial asymmetry, from fits of zero field muon spin relaxation data using an exponential relaxation function.

network of regular edge sharing tetrahedra. On heating, there is no evidence of any structural phase transition, confirming that the cubic symmetry is maintained up to room temperature, as shown in Fig. 6.

Muon spin relaxation measurements of local magnetic fields

In order to further probe the magnetic behavior of Ba_2MnMoO_6, μSR measurements were performed. Temperature dependent, zero field measurements can be fitted with an exponential function above 9.4 K, indicative of the paramagnetic behavior. At lower temperatures, there is a significant loss of asymmetry to a third of its initial value, but no oscillations are observed. This rapid depolarization of the muons is indicative of the muons oscillating on a timescale faster than can be detected at the ISIS pulsed muon source, due to strong local magnetic fields arising from ordering of moments within the sample. The data were fitted with a single exponential function over the entire temperature range. Data measured above and below T_N are shown in Fig. 6. The relaxation rate, λ, increases on cooling, to a sharp maximum at 7.9 K (Fig. 7), before decreasing to a constant but finite value of 0.57 μs, indicative of persistent spin dynamics. The peak in the muon spin relaxation rate occurs at a somewhat lower temperature than the transition temperatures observed by neutron diffraction. This effect may be expected for a technique probing an intermediate timescale, when the long-range ordering of the system is manifested as a gradual slowing down of the dynamics; as the dynamics of the system slow down on cooling, the timescale on which they appear static becomes longer. This is seen as an ordering transition at successfully lower temperatures as the timescale probed by the measurement technique increases. As a comparison, the μSR relaxation in the doped analog $Ba_2Nd_{0.3}Mn_{0.7}MoO_6$ was also measured. It shows a similar loss in the initial asymmetry, but over a broader temperature range, despite no evidence of the long-range magnetic order in either *d.c.* susceptibility or low temperature neutron powder diffraction measurements.[26]

DISCUSSION

Ba_2MnMoO_6 shows a magnetic behavior that shares the characteristics of the long-range antiferromagnetic order and the disordered character of a dynamic paramagnetic material. The magnetic Bragg peaks evident in neutron diffraction experiments indicate a configuration of magnetic moments that appear static and ordered to the diffracted neutron wave. Consideration of the lengthscale of diffraction and the speed of a thermal neutron with a de Broglie wavelength of ~2 Å suggests that the passage of a neutron wave through ten magnetic unit cells, a distance of ~160 Å, at a speed of 2000 m s^{-1} occurs over picosecond timescales. Under these conditions, all magnetic moments appear fully ordered below T_N of 9.37(7) K. However, at this temperature, muons indicate some disorder in the local magnetic field that persists until the sample is cooled to 7.9 K. Thus, in the range $7.9 < T/K < 9.37$, the magnetic Bragg scattering indicates a static, long range ordered antiferromagnetism, while the muons indicate spin dynamics that are gradually slowing through the timescale of the muon measurement as the thermal energy is reduced.

The clear signatures of magnetic transition occur at slightly different temperatures for neutron and muon measurements but are absent from the bulk *d.c.* susceptibility measurements. Here, the magnetization does not have the clear maximum that signifies spin cancellation due to antiferromagnetic ordering. This provides a stark contrast to the sharp maxima observed in the isostructural compounds Ba_2MnWO_6[28] and Ba_2MnTeO_6,[27] where the susceptibility maxima clearly indicate the temperatures at which magnetic Bragg peaks appear. Instead, Ba_2MnMoO_6 shows a subtle feature at 4 K, which implies a marginal, partial cancellation of the spins at this temperature.

The magnetic transition of Ba_2MnMoO_6 is unusual in other ways. The muon relaxation measurements of Ba_2MnWO_6[28] show a sharp loss of asymmetry at the 8.25 K transition temperature followed by a gradual increase, indicating the presence of persistent short-range correlations up to 30 K. Similarly, inelastic neutron scattering measurements on Ba_2MnTeO_6[27] show the presence of short range magnetic correlations persisting up to at least 109 K, well above the 20 K Néel temperature. By contrast, the muon relaxation measurements on Ba_2MnMoO_6 show that the internal magnetic field arising from ordering of the spins is lost at 7.9 K and there is no evidence of short range correlations above this transition.

Consideration of the unusual signatures of the magnetic transition in Ba_2MnMoO_6 led us to consider the exchange pathways that drive the magnetic ordering. If the antiferromagnetic coupling between next-nearest neighbors dominates, then it leads to collinear antiparallel ordering of a sub-lattice of Mn spins that compose one quarter of the magnetic species in a G-type ordering. The remaining spins are found on interpenetrating G-type ordered sublattices that form the apices of a tetrahedron. This approach delivers a distribution of magnetic Bragg scattering that is barely distinguishable from the type II structure previously suggested for Ba_2MnMoO_6 and identified in Ba_2MnWO_6. In the latter, inelastic neutron scattering measurements identified a finely balanced competition between nearest neighbor ($J = -0.080$ meV) and next-nearest neighbor coupling ($J = -0.076$ meV).[28] Given the similarities in the neutron Bragg scattering between these two models, it is likely that inelastic neutron scattering measurements are needed to discriminate between these two possibilities and provide insights into the nature of the ordered phase.

The magnetic susceptibility indicates that at higher temperatures, in the paramagnetic regime, strong antiferromagnetic coupling exists between the Mn^{2+} spins. Despite these strong correlations, magnetization measurements show that the spins remain largely uncompensated down to 2 K. This suggests that the static spin configuration identified in the neutron measurements may represent a snapshot of a magnetic state that is readily disrupted and possibly dynamic, under the conditions and timescale of a magnetic susceptibility measurement.

This strong technique dependence has some precedent in the observations of the pyrochlore $Tb_2Sn_2O_7$.[48] The coupling of the Tb^{3+} cations in this structure involves the $4f^8$ centers and so is weaker than the 3d mediated interactions of Ba_2MnMoO_6. The high temperature paramagnetic regime indicates that the weaker antiferromagnetic coupling in the frustrated lattice of $Tb_2Sn_2O_7$ is manifested in a lower Weiss constant, Θ, = −12 K. Neutron diffraction indicates that the magnetic moments become ordered below 0.87 K. However, the absence of any evidence of a magnetic

transition in the muon measurements below this temperature was taken as evidence of a non-static magnetic ground state. Our observations on Ba_2MnMoO_6 show that this de-coupling of magnetic transition temperatures can be observed in the frustrated *fcc* lattice. The stronger coupling lifts these effects into a more accessible temperature range and suggests that Ba_2MnMoO_6 may be a suitable system for probing these effects.

SUPPLEMENTARY MATERIAL

See the supplementary material for the crystal structure of Ba_2MnMoO_6 derived from Rietveld analyses against the D2B neutron diffraction data collected at 2 K, which is described in the Crystallographic Information File.

ACKNOWLEDGMENTS

This work was supported by the Universities of Strathclyde and Sheffield and awards from the EPSRC (Grant No. EP/H001751/1) and the Leverhulme Trust (Grant No. RPG-2017-109). O. M. is grateful for funding via the Leverhulme Trust Early Career Fellowship (Grant No. ECF-2021-170). We are grateful to Dr. E. Suard for assistance with the neutron diffraction experiments and Dr. M. Telling for assistance with the μSR measurements, and to the Institut Laue-Langevin, ISIS, and the Diamond Light Source for providing access to these facilities. Magnetic measurements were possible due to the kind support of the Shared Experimental Facilities of the Materials Research Laboratory at the University of California, Santa Barbara, supported by the MRSEC Program of the NSF under Award No. DMR 1121053, and the authors thank Professor Ram Seshadri at UCSB for his help and support. For the purpose of open access, the author has applied a Creative Commons Attribution (CC BY) license to the Author Accepted Manuscript version and this publication was supported by the University of Sheffield Institutional Open Access Fund. Data are available on request from the corresponding author (E.J. Cussen@Sheffield.ac.uk).

AUTHOR DECLARATIONS

Conflict of Interest

The authors have no conflicts to disclose.

Author Contributions

Fiona C. Coomer: Data curation (supporting); Formal analysis (lead); Investigation (equal); Methodology (equal); Writing – original draft (equal). **Heather M. Mutch**: Formal analysis (supporting); Investigation (supporting). **Otto Mustonen**: Investigation (supporting); Methodology (supporting); Supervision (supporting). **Charlotte Pughe**: Formal analysis (supporting); Investigation (supporting); Methodology (supporting). **Serena A. Cussen**: Formal analysis (supporting); Investigation (supporting); Validation (supporting). **Silvia Ramos**: Formal analysis (equal); Methodology (supporting); Writing – original draft (supporting). **Adrian D. Hillier**: Formal analysis (equal); Investigation (supporting); Methodology (supporting); Writing – original draft (supporting). **Edmund J. Cussen**: Conceptualization (equal); Formal analysis (equal); Funding acquisition (lead); Project administration (lead); Supervision (lead); Writing – original draft (equal); Writing – review & editing (lead).

DATA AVAILABILITY

The data that support the findings of this study are available from the corresponding author upon reasonable request.

REFERENCES

[1] J. E. Greedan, J. Mater. Chem. **11**, 37 (2001).
[2] A. L. Goodwin, M. G. Tucker, M. T. Dove, and D. A. Keen, Phys. Rev. Lett. **96**, 047209 (2006).
[3] A. Harrison, J. Phys.: Condens. Matter **16**, S553 (2004).
[4] T. Aharen, J. E. Greedan, C. A. Bridges, A. A. Aczel, J. Rodriguez, G. MacDougall, G. M. Luke, T. Imai, V. K. Michaelis, S. Kroeker, H. Zhou, C. R. Wiebe, and L. M. D. Cranswick, Phys. Rev. B **81**, 224409 (2010).
[5] T. Aharen, J. E. Greedan, C. A. Bridges, A. A. Aczel, J. Rodriguez, G. MacDougall, G. M. Luke, V. K. Michaelis, S. Kroeker, C. R. Wiebe, H. D. Zhou, and L. M. D. Cranswick, Phys. Rev. B **81**, 064436 (2010).
[6] S. T. Bramwell, S. R. Giblin, S. Calder, R. Aldus, D. Prabhakaran, and T. Fennell, Nature **461**, 956 (2009).
[7] S. Calder, X. Ke, F. Bert, A. Amato, C. Baines, C. Carboni, R. J. Cava, A. Daoud-Aladine, P. Deen, T. Fennell, A. D. Hillier, H. Karunadasa, J. W. Taylor, P. Mendels, P. Schiffer, and S. T. Bramwell, Phys. Rev. B **81**, 064425 (2010).
[8] M. Yoshida, M. Takigawa, S. Kramer, S. Mukhopadhyay, M. Horvatic, C. Berthier, H. Yoshida, Y. Okamoto, and Z. Hiroi, J. Phys. Soc. Jpn. **81**, 024703 (2012).
[9] P. W. Anderson, Mater. Res. Bull. **8**, 153 (1973).
[10] T.-H. Han, J. S. Helton, S. Chu, D. G. Nocera, J. A. Rodriguez-Rivera, C. Broholm, and Y. S. Lee, Nature **492**, 406 (2012).
[11] J. S. Gardner, S. R. Dunsiger, B. D. Gaulin, M. J. P. Gingras, J. E. Greedan, R. F. Kiefl, M. D. Lumsden, W. A. MacFarlane, N. P. Raju, J. E. Sonier, I. Swainson, and Z. Tun, Phys. Rev. Lett. **82**, 1012 (1999).
[12] J. E. Greedan, D. Gout, A. D. Lozano-Gorrin, S. Derahkshan, T. Proffen, H. J. Kim, E. Bozin, and S. J. L. Billinge, Phys. Rev. B **79**, 014427 (2009).
[13] J. E. Greedan, S. Derakhshan, F. Ramezanipour, J. Siewenie, and T. Proffen, J. Phys.: Condens. Matter **23**, 164213 (2011).
[14] A. S. Wills and W. G. Bisson, J. Phys.: Condens. Matter **23**, 164206 (2011).
[15] A. P. Ramirez, A. Hayashi, R. J. Cava, R. Siddharthan, and B. S. Shastry, Nature **399**, 333 (1999).
[16] S. T. Bramwell, M. J. P. Gingras, and J. P. Michael, Science **294**, 1495 (2001).
[17] M. A. de Vries, A. C. McLaughlin, and J.-W. G. Bos, Phys. Rev. Lett. **104**, 177202 (2010).
[18] F. C. Coomer and E. J. Cussen, J. Phys.: Condens. Matter **25**, 082202 (2013).
[19] J. Romhanyi, L. Balents, and G. Jackeli, Phys. Rev. Lett. **118**, 217202 (2017).
[20] O. H. J. Mustonen, H. M. Mutch, H. C. Walker, P. J. Baker, F. C. Coomer, R. S. Perry, C. Pughe, G. B. G. Stenning, C. Liu, S. E. Dutton, and E. J. Cussen, npj Quantum Mater. **7**, 74 (2022).
[21] P. M. Woodward, Acta Cryst. **53**, 32 (1997).
[22] H. Ishizuka and L. Balents, Phys. Rev. B **90**, 184422 (2014).
[23] Y. Kasahara, Y. Takeuchi, T. Itou, R. H. Zadik, Y. Takabayashi, A. Y. Ganin, D. Arcon, M. J. Rosseinsky, K. Prassides, and Y. Iwasa, Phys. Rev. B **90**, 014413 (2014).
[24] B. H. Yan, A. K. Paul, S. Kanungo, M. Reehuis, A. Hoser, D. M. Toebbens, W. Schnelle, R. C. Williams, T. Lancaster, F. Xiao, J. S. Moller, S. J. Blundell, W. Hayes, C. Felser, and M. Jansen, Phys. Rev. Lett. **112**, 147202 (2014).
[25] E. J. Cussen, D. R. Lynham, and J. Rogers, Chem. Mater. **18**, 2855 (2006).
[26] F. C. Coomer and E. J. Cussen, Inorg. Chem. **53**, 746 (2014).
[27] O. H. J. Mustonen, C. E. Pughe, H. C. Walker, H. M. Mutch, G. B. G. Stenning, F. C. Coomer, and E. J. Cussen, Chem. Mater. **32**, 7070 (2020).
[28] H. Mutch, O. Mustonen, H. C. Walker, P. J. Baker, G. B. G. Stenning, F. C. Coomer, and E. J. Cussen, Phys. Rev. Mater. **4**, 014408 (2020).

[29] J. I. Kaplan, J. Chem. Phys. **22**, 1709 (1954).
[30] F. Keffer and W. O'Sullivan, Phys. Rev. **108**, 637 (1957).
[31] C. G. Shull and J. S. Smart, Phys. Rev. **76**, 1256 (1949).
[32] C. G. Shull, W. A. Strauser, and E. O. Wollan, Phys. Rev. **83**, 333 (1951).
[33] W. L. Roth, Phys. Rev. **110**, 1333 (1958).
[34] S. Lv, X. Liu, H. Li, Z. Wu, and J. Meng, Comput. Mater. Sci. **49**, 266 (2010).
[35] M. J. Martínez-Lope, J. A. Alonso, and M. T. Casais, Z. Naturforsch., B: J. Chem. Sci. **58**, 571 (2003).
[36] C. P. Khattak, D. E. Cox, and F. F. Y. Wang, J. Solid State Chem. **17**, 323 (1976).
[37] A. C. Larson and R. B. von Dreele, *General Structure Analysis System (GSAS)* (Los Alamos National Laboratories, Los Alamos, NM, 1990).
[38] B. H. Toby, J. Appl. Crystallogr. **34**, 210 (2001).
[39] B. Ravel and M. Newville, J. Synchrotron Radiat. **12**, 537 (2005).
[40] B. Ravel, J. Alloys Compd. **401**, 118 (2005).
[41] O. Arnold, J. C. Bilheux, J. M. Borreguero, A. Buts, S. I. Campbell, L. Chapon, M. Doucet, N. Draper, R. Ferraz Leal, M. A. Gigg, V. E. Lynch, A. Markvardsen, D. J. Mikkelson, R. L. Mikkelson, R. Miller, K. Palmen, P. Parker, G. Passos, T. G. Perring, P. F. Peterson, S. Ren, M. A. Reuter, A. T. Savici, J. W. Taylor, R. J. Taylor, R. Tolchenov, W. Zhou, and J. Zikovsky, Nucl. Instrum. Methods Phys. Res., Sect. A **764**, 156 (2014).
[42] R. D. Shannon, Acta Cryst. **32**, 751 (1976).
[43] D. Herrmann-Ronzaud, P. Burlet, and J. Rossat-Mignod, J. Phys. C: Solid State Phys. **11**, 2123 (1978).
[44] J. W. G. Bos and J. P. Attfield, Phys. Rev. B **70**, 174434 (2004).
[45] R. Morrow, R. Mishra, O. D. Restrepo, M. R. Ball, W. Windl, S. Wurmehl, U. Stockert, B. Büchner, and P. M. Woodward, J. Am. Chem. Soc. **135**, 18824 (2013).
[46] P. W. Anderson, Phys. Rev. **79**, 705 (1950).
[47] M. F. Collins, *Magnetic Critical Scattering* (Oxford University Press Inc., New York, 1989).
[48] P. Dalmas de Réotier, A. Yaouanc, L. Keller, A. Cervellino, B. Roessli, C. Baines, A. Forget, C. Vaju, P. C. M. Gubbens, A. Amato, and P. J. C. King, Phys. Rev. Lett. **96**, 127202 (2006).